Electronic Supplementary Material (ESI) for Journal of Materials Chemistry A.

Ultra-Thin, Flexible, Low-Cost and Scalable Gas Diffusion Layer Made by Carbon Nanotube for High Performance Fuel Cell

Jun Wei,[1,2] Fandi Ning,[1] Chuang Bai,[1] Ting Zhang,[1] Guanbin Lu,[1] Huihui Wang,[1] Yali Li,[1] Yangbin Shen,[3] Xuwei Fu,[1,2] Qingwen Li,[1] Hehua Jin,[1] and Xiaochun Zhou[1,4]*

1. Division of Advanced Nanomaterials, Suzhou Institute of Nano-tech and Nano-bionics, Chinese Academy of Sciences (CAS), Suzhou 215123, China
2. Nano Science and Technology Institute, University of Science and Technology of China, Suzhou 215123, China
3. Institute of Materials Science and Devices, Suzhou University of Science and Technology, Suzhou 215009, China
4. Key Lab of Nanodevices and Applications, Suzhou Institute of Nano-Tech and Nano-Bionics, Chinese Academy of Sciences (CAS), Suzhou 215123, China.

Email: xczhou2013@sinano.ac.cn

Table of contents

SI-1. Chemicals and Experimental details

Chemicals

All chemicals were commercial and used without further purification unless specified. Ethanol (C_2H_5OH, Tianjin Baishi Chemical Industry, Co., Ltd, >99.7%), acetone (CH_3COCH_3, Sinopharm Chemical Reagent, Co., Ltd. >98%), carbon nanotubes powder (Nanjing XFNANO Tech, Co., Ltd. >99%), carbon nanotubes film (Suzhou Jiedi NANO Tech, Co., Ltd. >99%), sodium dodecylbenzene sulfonate (SDBS, Tianjin BASF chemical, Co., Ltd.), poly tetrafluoroethylene (PTFE, USA-Sigma-Aldrich, Co., Ltd.), sodium hydroxide (NaOH, Sinopharm Chemical Reagent, Co., Ltd, >96%), hydrogen peroxide(Na_2O_2, Sinopharm Chemical Reagent, Co., Ltd, >60%), isopropyl alcohol ($CH_3CHOHCH_3$, Sinopharm Chemical Reagent, Co., Ltd. >98%), 70% Pt/C (HiSPEC13100, Johnson Matthey, Co., Ltd.). The remaining chemicals were of analytical grade and commercially available from Shanghai Chemical Reagent Co, Ltd.

Preparation of CNT membrane with ordered porous structures

Porous diffused layer basement membrane with laser perforation is applied in the preparation of diffused layer basement.[1] Laser hole drilling on the carbon nanotube film produced a uniform aperture, evenly arranged array of holes. Adjust the pore size and the distance between two neighbor pores by adjusting the machine current and the number of laser drilling. Typically, the pore size is 52 μm, and the distance between two neighbor pores is 107 μm.

Preparation of the new GDL

Preparation of carbon nanotubes dispersion. The CNT powder dispersion was prepared just as reported in our previous work. In detail, 0.1 mg mL^{-1} CNT powder, 1 mg mL^{-1} sodium dodecyl benzene sulfonate and deionized water were mixed and sonicated for 10 h under a power of 2 kW.

Electroplating. The electrical conductivity of carbon nanotubes was enhanced by the electrodeposition of highly conductive metals on carbon nanotubes. A certain amount of gold dissolved in aqua regal or chloroauric acid as electrolyte. CNT membrane was as the working electrode; Ag/AgCl was as the reference electrode; platinum or gold was as the counter electrode. Controlling the plating current and plating time to make the gold plating amount at 0.3 mg cm^{-2}.

Prepare the MPL. Mix a certain amount of carbon nanotube dispersion and PTFE emulsion, and the content of carbon nanotube and PTFE were 35% and 65% respectively. Ultrasound the mixture in the ultrasonic cleaning machine for 5 minutes to make it evenly. The perforated carbon nanotube film was used as a base layer, and the prepared mixture was poured into a suction filter bottle. After the end of the suction filtration, the obtained new GDL were naturally dried and were baked at 350 °C for 30 min, cooled to room temperature.

Preparation of MEA

The MEA was prepared and used in this study as follows: The catalyst loading was 0.5 mg cm^{-2} for both cathode and anode. Nafion 211 membrane was hot pressed with two electrodes at a pressure of 40 Kg_f cm^{-2} and temperature of 130 ℃ for 2 min.

Characterizations

The cell operating test conditions. The operating conditions in our performance test were dry air and hydrogen through a gas washer bottle at the ambient temperature (20°C) and pressure. The pure hydrogen was prepared from a hydrogen generator.

Experimental equipment. The morphology and structure of the CNT membrane materials and new GDL were characterized by using an SEM. The square resistance was measured by using the four-point probe technique. The electrochemical performance was measured by an electrochemical work station (CS), and copper wires were connected to the electrodes to measure the current. Universal tensile machine test CNT film and new GDL tensile strength. The pore size and specific surface area of the material were characterized by BET.

Optimizations of preparation and working conditions

In order to improve the performance of the flexible PEMFC, a series of optimizations have been carried out. Firstly, the load of CNT powder was optimized, secondly, a series of studies on the PTFE content in the GDL were carried out to obtain the optimal value.

SI-2. Thickness ratio of GDL in fuel cell

✧ Maximum ratio of GDL

Nafion211 thickness: 0.025 mm

Bipolar plate thickness: 1 mm

GDL thickness: 0.4 mm

Catalytic layer thickness: 0.007 mm

Thickness ratio of GDL: $\frac{GDL\times2}{GDL\times2+bipolar\ plate+membrane+Catalytic\ layer\times2}=\frac{0.4\times2}{1+0.4\times2+0.025+0.014}$=43.5%

✧ Minimum ratio of GDL

Nafion115 thickness: 0.125 mm

Bipolar plate thickness: 3 mm

GDL thickness: 0.1 mm

Catalytic layer thickness: 0.007 mm

Thickness ratio of GDL: $\frac{GDL\times2}{GDL\times2+bipolar\ plate+membrane+\text{Catalytic layer}\times2}=\frac{0.1\times2}{3+0.1\times2+0.125+0.014}$=6.0%

SI-3. CNT membrane and new GDL stress versus strain

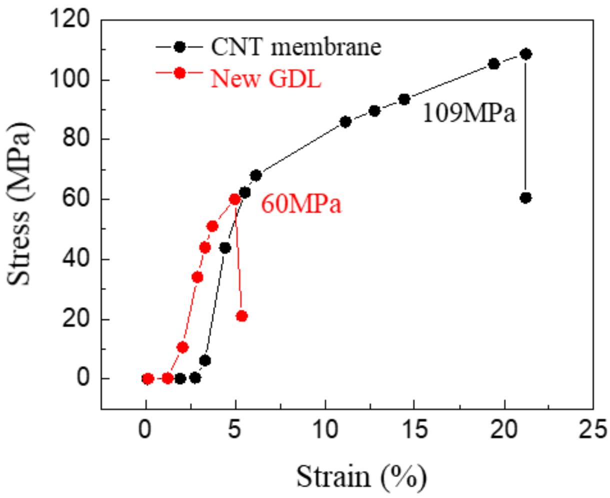

Figure S1. CNT membrane and new GDL stress versus strain. The tensile stress of the CNT membrane could reach 109 MPa, and it will decrease dramatically after treating with laser drill. The tensile stress will return to 60MPa when preparing the new GDL.

SI-4. Optical photo of MWCNT powder dispersion.

Figure S2. Optical photo of MWCNT powder dispersion. The concentration of the MWCNT powder dispersion is 0.1 mg mL^{-1}. MWCNT powder dispersion is a black homogeneous dispersion solution with no obvious precipitation.

SI-5. Gas permeability test

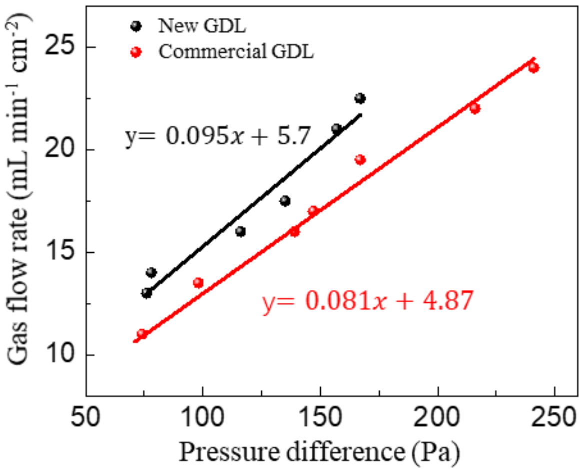

Figure S3. New GDL gas and commercial GDL gas permeability test. As is shown in the **Error! Not a valid bookmark self-reference.** under 20℃ and atmospheric pressure test conditions, the gas permeability of New GDL was 9630 mL min^{-1} cm^{-2} atm^{-1}. The commercial GDL had a gas permeability of 8210 mL min^{-1} cm^{-2} atm^{-1}.

SI-6. Flexibility test

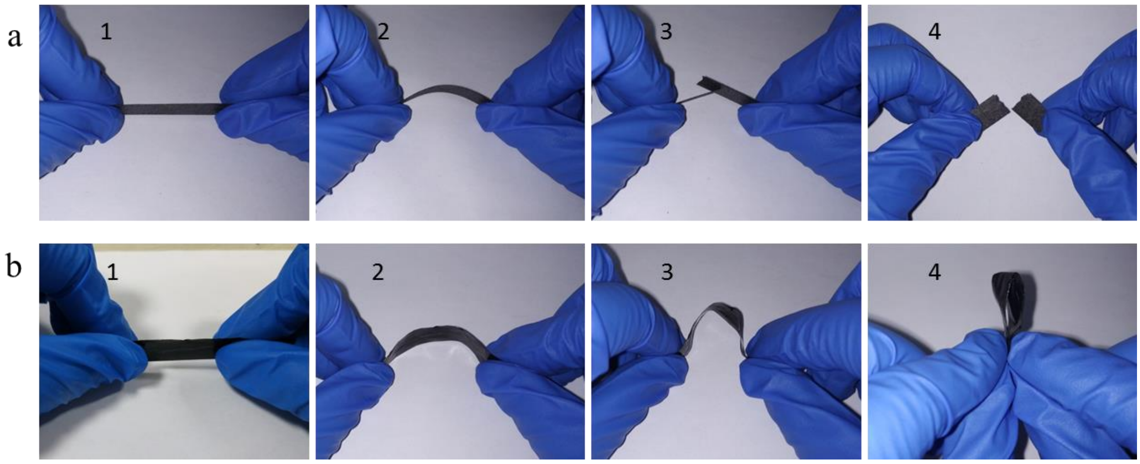

Figure S4. With the change of bending Angle, commercial GDL and new GDL show different results. (a) TGP-H-060. (b) New GDL. The commercial GDL was cracked when the bending angle reached to 30°. Given a little pressure, the commercial GDL was completely broken as shown in a-3. While the new GDL could not be destroyed even the angle reached over 180°.

SI-7. SEM characterization of the new GDL and commercial GDL after hot pressing

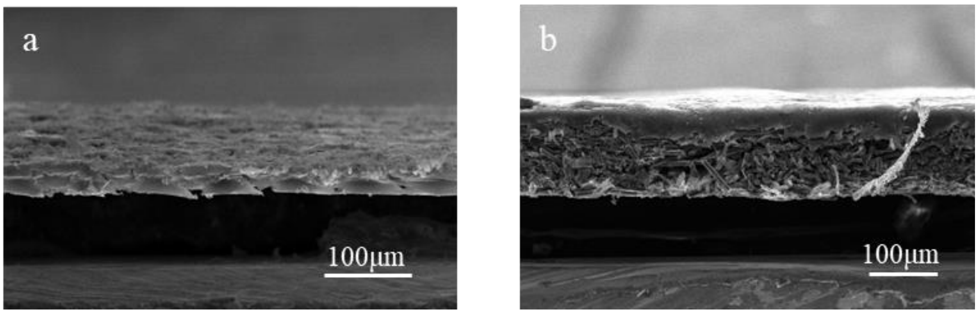

Figure S5. SEM characterization of the new GDL and commercial GDL after hot pressing. (a)New GDL after hot pressing. (b) Commercial GDL after hot pressing. As was shown in the SEM, the structure of the new GDL nearly unchanged compared to the commercial carbonized paper after hot pressing. The porosity of commercial GDL was less than before, and the pore size distribution was uneven when treated with hot press.

SI-8. Weight-specific power density and volume-specific power density

Thickness: 118 μm

Working area: 5 cm^2

Volume: 1.2 cm (width) × 5.2cm (length) ×0.00118cm (thickness) = 0.0736 cm^3

Weight: 0.119 g

Peak power density: 230 mW cm^{-2}

Volume-specific power density $=\frac{5\times\text{peak power density}}{V}=15600\ \text{W L}^{-1}$

Weight-specific power density $= \frac{5\times\text{peak power density}}{m}= 9660\ \text{W kg}^{-1}$

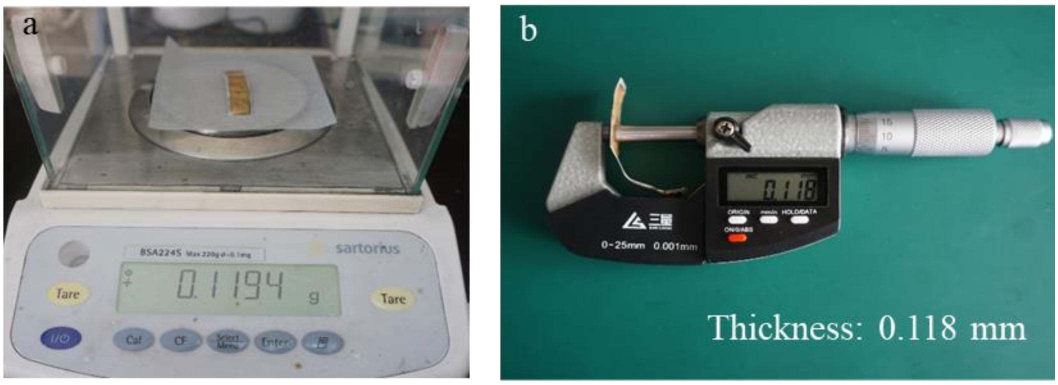

Figure S6. The calculation process and 1×5 cm^2 fuel cell quality and thickness photos. (a) Fuel cell weight. (b) Fuel cell thickness. As is shown in the picture and the calculation progress of volume-specific power density and weight-specific power density, the final calculated volume-specific power density is 15600 W L^{-1} and weight-specific power density is 9660 W kg^{-1}.

SI-9. Flexibility test of new GDL fuel cell

Fuel cell thickness: 118 μm

Fuel cell working area: 5 cm^2

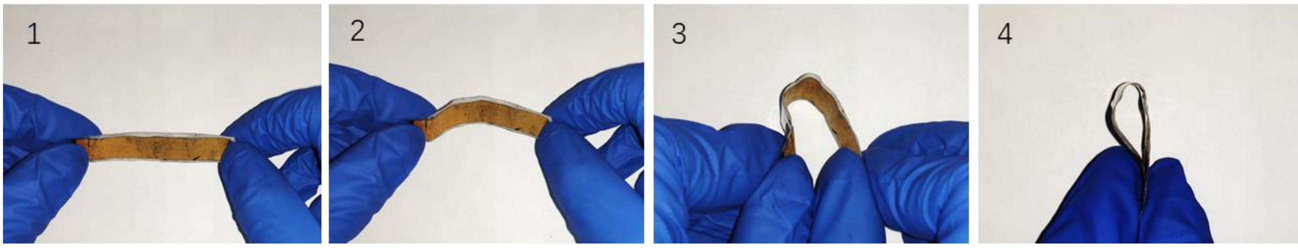

Figure S7. Flexibility test at different bending angles for the fuel cell with new GDL. As shown in the photo, the fuel cell with new GDL is always intact and in good condition, without breaking or interface peeling.

SI-10. Lifetime test of fuel cell with new GDL

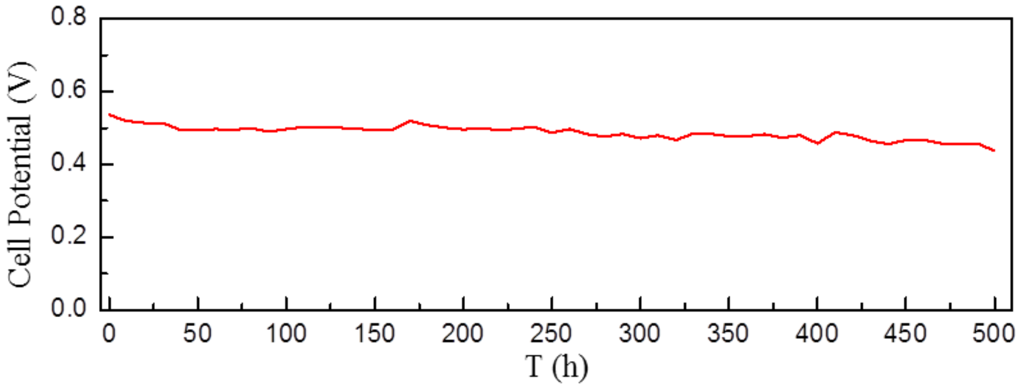

Figure S8. Lifetime test of fuel cell with new GDL. The effective area of fuel cell with the new GDL was 1 cm^2. The new GDL could stably work for at least 500 hours under the constant 50 mA current, normal pressure and temperature.

SI-11. The contact angle changes with the change of PTFE content

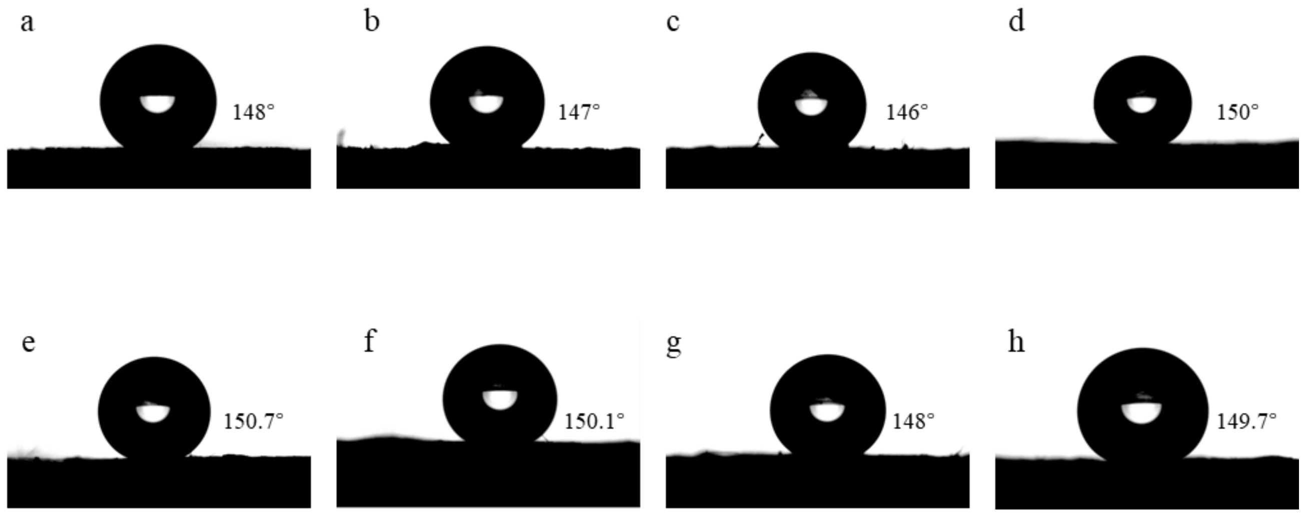

Figure S9. The contact Angle changes with the change of PTFE content. The amount of PTFE was (a) 26.7%. (b) 42.2%. (c) 52.2%. (d) 59.3%. (e) 65%. (f) 72.8%. (g) 77.8%. (h) 81.2%.

SI-12. The contact angle changes with the change of CNT powder content

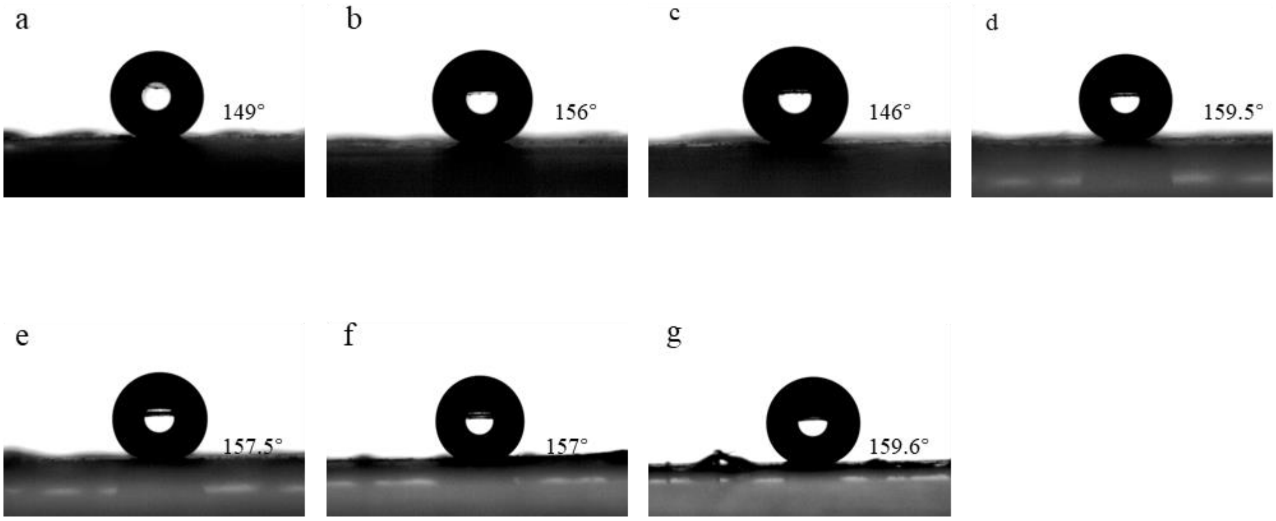

Figure S10. The contact Angle changes with the change of CNT powder content. The amount of CNT powder was (a) 16.8%. (b) 21.2%. (c) 28.7%. (d) 35%. (e) 40.2%. (f) 44.6%. (g) 46.6%.

SI-13. Comparison of commercial GDL and new GDL

✧ **Parameters for new GDL fuel cell:**

MEA thickness: 0.089 mm

Bipolar plate thickness: 1 mm

Fuel cell thickness: 1.089 mm

Peak power density: 840 mW cm^{-2}

✧ **Parameters for commercial GDL fuel cell:**

MEA thickness: 0.35 mm

Bipolar plate thickness: 1 mm

Fuel cell thickness: 1.35 mm

Peak power density: 634 mW cm^{-2}

Fuel cell thickness reduction in traditional testing:

$$\frac{\textit{Commercial GDL fuel cell}\ \text{thickness} - \textit{New GDL fuel cell}\ \text{thickness}}{\textit{Commercial GDL fuel cell}\ \text{thickness}} = \frac{1.35-1.089}{1.35} = 19.3\%$$

Fuel cell performance improvement in traditional testing:

$$\frac{\textit{Commercial GDL fuel cell}\ \text{Pmax} - \textit{New GDL fuel cell}\ \text{Pmax}}{\textit{Commercial GDL fuel cell}\ \text{Pmax}} = \frac{840-634}{634} = 32.5\%$$

PEMFC volume-specific power density improvement in traditional testing：

$$\frac{\textit{Commercial GDL fuel cell}\ \text{volume-specific power density} - \textit{New GDL fuel cell}\ \text{volume-specific power density}}{\textit{Commercial GDL fuel cell}\ \text{volume-specific power density}} =$$

$$\frac{771.3-469.6}{469.6} = 64.2\%$$

SI-14. Inner resistances of the fuel cells

The discharge curve of the PEMFC with new GDL is flatter, comparing to the slope of the PEMFC with commercial GDL. The flatter slope of the PEMFC with new GDL indicates a low inner resistance (0.16 Ω in **Figure S11**), which is mainly attributed to the advantages of low contact resistance, and high flexibility etc.

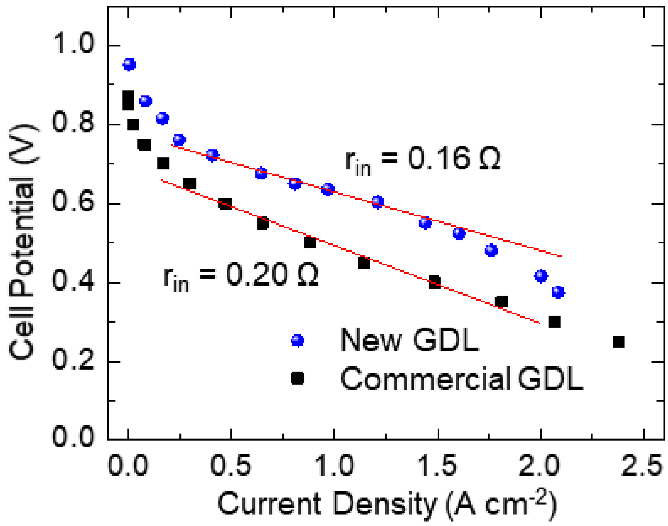

Figure S11. Polarization curves for our new GDL and commercial GDL measured by traditional hydrogen-oxygen PEMFC. The inner resistances of the fuel cells are obtained by a linear fitting during the working current density from about 0.5 to 1.5 A.

SI-15. Effect of pore size and distance between neighboring pores

The size of the drilled pores and the distance between neighboring pores could influence the performance of the new GDL. **Figure S12**a shows that the pore size and the relation of the distance between neighboring pores. **Figure S12**b shows that the pore size has a strong effect on the performance of the new GDL. The maximum performance appears at the pore size of 52 μm as shown in **Figure S12**b. Therefore, the pore size (2R) has an optimum value. Since the distance between neighboring pores equals the pore size (2R), the optimum value is also for the distance.

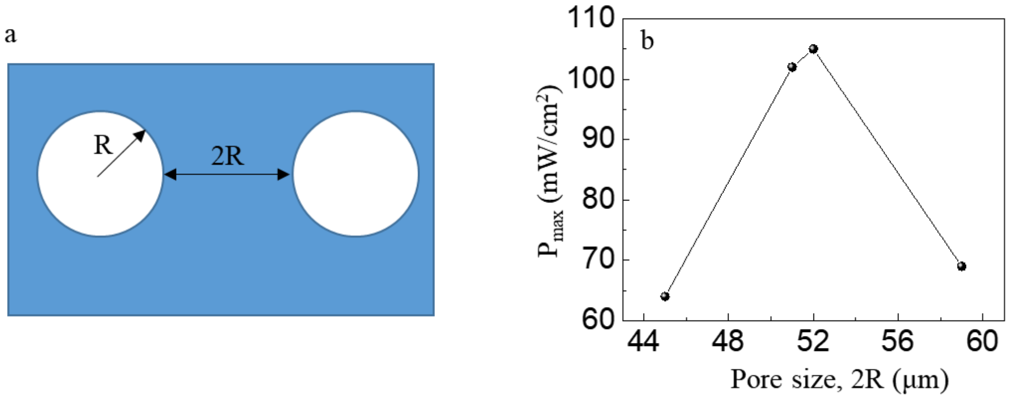

Figure S12. Effect of pore size and distance between neighboring pores on the performance of the new GDL. (a) Schematic of pore size and distance between neighboring pores. (b) Effect of pore size (distance) on the performance of the new GDL.

SI-16. The development of volume-specific power density in recent years

Table S1. Details volume-specific power density in recent years

Year	**volume-specific power density ($W\ L^{-1}$)**	**reference**
1997	300	[2]
2004	500	[3]
2006	360	[4]
2008	3107	[5]
2010	3040.9	[6]
2010	2715.94	[7]
2012	5764.0	[8]
2016	3100	[9]
2017	5190	[1]
2019	15600	This work

SI-17. Composition of commercial GDL and the new GDL in this paper

Table S2. Details of GDL comparison.

Parameters	**New GDL in this work**	**Commercial GDL**
Gas permeability (mL min^{-1} cm^{-2} atm^{-1})	9630	8210
Conductivity (s m^{-1})	23450	16500
Thickness (mm)	0.089	0.197
Porosity (%)	80	78

SI-18. Comparison of commercial GDL and new GDL in fuel cell performance

Table S3. Details of fuel cell comparison.

Parameters	New GDL fuel cell in this paper	Commercial GDL fuel cell[1]
Working area (cm^2)	1×5	1×1
Quality (g)	0.0238	0.065
Volume (cm^3)	0.0147	0.028
Thickness (mm)	0.118	0.22
Specific area power density (mW cm^{-2})	230	145.2
Specific volume power densities (W L^{-1})	15600	5190
Specific weight power densities (W kg^{-1})	9660	2230

SI-19. Comparison of fuel cell performance

Moreover, the fuel cell performance 840 mW cm^{-2} with new GDL in Figure 4 is actually at the middle level comparing to the results in literatures (refer **Table S4**).

Table S4. Comparison of fuel cell performance

Index	Maximum power density (mW cm^{-2})	Operating temperature (°C)	Gas feed	Ref.
1	106	80	H_2/air	[10]
2	800	70	H_2/O_2	[11]
3	320	90	H_2/O_2	[12]
4	1100	80	H_2/air	[13]
5	1220.2	180	H_2/O_2	[14]
6	559	160	H_2/O_2	[15]
7	1067	70	H_2/O_2	[16]
8	721.7	60	H_2/O_2	[17]
9	536	60	H_2/O_2	[18]
10	840	80	H_2/O_2	**This work**

SI-20. References

1 F. D. Ning, X. D. He, Y. B. Shen, H. H. Jin, Q. W. Li, D. Li, S. P. Li, Y. L. Zhan, Y. Du, J. J. Jiang, H. Yang and X. C. Zhou, *Acs Nano*, 2017, **11**, 5982-5991.

2 C. E. Thomas, I. F. Kuhn, B. D. James, F. D. Lomax and G. N. Baum, *Int. J. Hydrogen Energy*, 1998, **23**, 507-516.

3 J. S. Cooper, *J. Power Sources*, 2004, **129**, 152-169.

4 J. Y. Kim, O. J. Kwon, S. M. Hwang, M. S. Kang and J. J. Kim, *J. Power Sources*, 2006, **161**, 432-436.

5 S. H. Liao, C. Y. Yen, C. C. Weng, Y. F. Lin, C. C. M. Ma, C. H. Yang, M. C. Tsai, M. Y. Yen, M. C. Hsiao, S. J. Lee, X. F. Xie and Y. H. Hsiao, *J. Power Sources*, 2008, **185**, 1225-1232.

6 P. Y. Yi, L. F. Peng, L. Z. Feng, P. Gan and X. M. Lai, *J. Power Sources*, 2010, **195**, 7061-7066.

7 P. Y. Yi, L. F. Peng, X. M. Lai, D. A. Liu and J. Ni, *Fuel Cells*, 2010, **10**, 111-117.

8 P. Y. Yi, L. F. Peng, X. M. Lai, Z. Q. Lin and J. Ni, *Fuel Cells*, 2012, **12**, 1019-1026.

9 C. Wang, S. B. Wang, L. F. Peng, J. L. Zhang, Z. G. Shao, J. Huang, C. W. Sun, M. G. Ouyang and X. M. He, *Energies*, 2016, **9**, 39.

10 S. K. Babu, R. W. Atkinson, A. B. Papandrew and S. Litster, *ChemElectroChem*, 2015, **2**, 1752-1759.

11 Z. Xia, S. Wang, L. Jiang, H. Sun, S. Liu, X. Fu, B. Zhang, D. Sheng Su, J. Wang and G. Sun, *Scientific reports*, 2015, **5**, 16100.

12 M. Aizawa, H. Gyoten, A. Salah and X. Liu, *J. Electrochem. Soc.*, 2010, **157**, B1844.

13 A. Kongkanand and M. F. Mathias, *The Journal of Physical Chemistry Letters*, 2016, **7**, 1127-1137.

14 H. Bai, H. Peng, Y. Xiang, J. Zhang, H. Wang, S. Lu and L. Zhuang, *Journal of Power Sources*, 2019, **443**.

15 H. Bai, H. Wang, J. Zhang, J. Zhang, S. Lu and Y. Xiang, *Journal of Membrane Science*, 2019, **592**.

16 S. Hanif, X. Shi, N. Iqbal, T. Noor, R. Anwar and A. M. Kannan, *Appl. Catal. B-Environ.*, 2019, **258**.

17 X. Q. Gao, H. M. Yu, B. W. Qin, J. Jia, J. K. Hao, F. Xie and Z. G. Shao, *Polym. Chem.*, 2019, **10**, 1894-1903.

18 R. Singh, M. K. Singh, S. Bhartiya, A. Singh, D. K. Kohli, P. C. Ghosh, S. Meenakshi and P. K. Gupta, *International Journal of Hydrogen Energy*, 2017, **42**, 11110-11117.